Accepted Manuscript

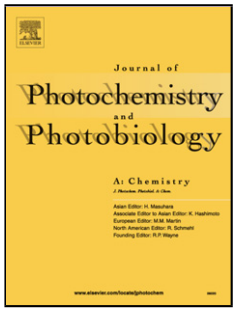

Title: A novel water-soluble tetranuclear copper (II) Schiff base cluster bridged by 2, 6-bis-[(2-hydroxyethylimino)methyl]-4-methylphenol in interaction with BSA: synthesis, X-ray crystallography, docking and cytotoxicity studies

Authors: Zahra Asadi, Maryam Golchin, Vaclav Eigner, Michal Dusek, Zahra Amirghofran

PII: S1010-6030(18)30249-1
DOI: https://doi.org/10.1016/j.jphotochem.2018.05.016
Reference: JPC 11286

To appear in: *Journal of Photochemistry and Photobiology A: Chemistry*

Received date: 21-2-2018
Revised date: 12-5-2018
Accepted date: 12-5-2018

Please cite this article as: Asadi Z, Golchin M, Eigner V, Dusek M, Amirghofran Z, A novel water-soluble tetranuclear copper (II) Schiff base cluster bridged by 2, 6-bis-[(2-hydroxyethylimino)methyl]-4-methylphenol in interaction with BSA: synthesis, X-ray crystallography, docking and cytotoxicity studies, *Journal of Photochemistry and Photobiology, A: Chemistry* (2010), https://doi.org/10.1016/j.jphotochem.2018.05.016

A novel water-soluble tetranuclear copper (II) Schiff base cluster bridged by 2, 6-bis-[(2-hydroxyethylimino)methyl]-4-methylphenol in interaction with BSA: synthesis, X-ray crystallography, docking and cytotoxicity studies

Zahra Asadi*[a], Maryam Golchin[a], Vaclav Eigner[b], Michal Dusek[b], Zahra Amirghofran[c]

a) Department of Chemistry, College of Sciences, Shiraz University, Shiraz 71454, Iran

b) Institute of Physics ASCR, v.v.i, Na Slovance 2, 182 21 Prague, Czech Republic

c) Department of Immunology and Autoimmune Diseases Research Center, Shiraz University of Medical Sciences, Shiraz 71454, Iran

Graphical Abstract

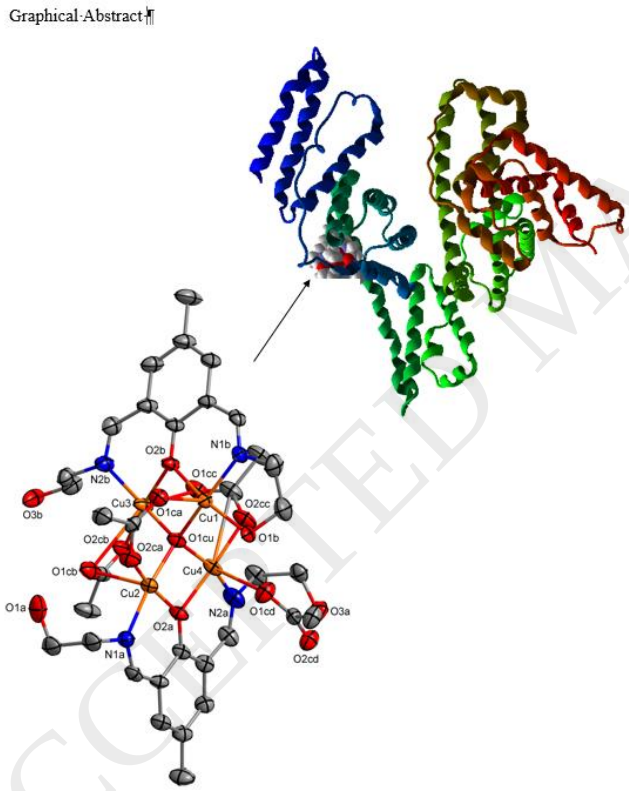

Highlights

- A water-soluble tetranuclear copper (II) Schiff base complex bridged by 2,6-bis-[(2-hydroxyethylimino)methyl]-4-methylphenol, namely $[Cu_4(L^1)_2(O)(OAc)_4].2H_2O$ was synthesized.
- The interaction with bovine serum albumin (BSA) was assessed.
- In vitro cytotoxicity against A549, Jurkat and Raji cell lines by MTT assay was done.
- Theoretical docking studies were investigated.

Abstract

A water-soluble tetranuclear copper (II) Schiff base complex bridged by 2,6-bis-[(2-hydroxyethylimino)methyl]-4-methylphenol, namely $[Cu_4(L^1)_2(O)(OAc)_4].2H_2O$ was synthesized. The complex was characterized by ^{1}HNMR, FT-IR, elemental analyses and single-crystal X-ray diffraction. The crystal structure analyses revealed that four Cu atoms were located around a central O atom in a distorted tetrahedral geometry. Beside the two ligands, four acetates also bridged the four Cu atoms. The interaction of the complex with Bovine serum albumin (BSA) was explored by absorption and emission titration methods the calculated binding constants revealed high affinity of the complex to BSA. The antitumor activity of the complex against Jurkat, Raji and A549 cell lines was assessed by the MTT colorimetric method. A strong activity against the cultured tumor cells was observed which makes the complex a possible candidate as an anticancer agent. Further investigation of the BSA-complex interactions was done by docking studies.

Keywords: tetranuclear copper (II) Schiff base complex; bovine serum albumin; docking; cytotoxicity.

Introduction

In recent years, research of the poly-nuclear complexes has a rapid development. Beside the fascinating molecular architecture, their applications including catalysis, fluorescence, gas storage, and biological activity are also attractive [1]. Schiff base ligands which contain alkoxo and phenoxo groups can bridge metal atoms in different modes and produce mononuclear, dinuclear or tetranuclear complexes [1]. A phenolato ion can bridge two Cu(II) centers and in this case the coordination number of each Cu(II) center range from 4 to 6 which is typical for

the coordination chemistry of Cu(II) [2]. Special attention has been focused on the discrete tetranuclear clusters, cubane-like oxygen-bridged Cu_4O_4 polynuclear complexes [3-6].

Copper, among the transition metals, is a biologically active one. The accessible redox potentials of copper complexes and their combination with dioxygen or hydrogen peroxide make them an effective DNA-cleavage agent through oxidative pathways. Multinuclear complexes have been used in order to increase the selectivity and efficiency of them as metallo-nuclease, due to cooperative effects between the metal centers [7].

Recently, the catecholase activity of dicopper(II) complexes with organic blocking ligands have been reported. Some copper(II) mononuclear complexes also exhibit this property. In 1998 the crystal structure of the catechol oxidase was determined; demonstrating the active site of a hydroxo-bridegd dicopper(II) center which coordinated to three histidine nitrogens [8].

Metal complexes and metal ions can transport through proteins in the blood stream. This property is important because many drugs including anticoagulants, anti-inflammatory, tranquilizers, and general anesthetics are delivered in the blood through combination with albumin [9]. Thus metal complexes that can bind to protein or DNA under physiological condition are interesting in designing the metal based drugs. Among them, water-soluble, inert and stable complexes, which contain spectroscopically active metal centers, are used as probes for biological systems. For example, copper complexes are good candidates for replacing platinum drugs and reveal better cancer inhibiting activity [10-15]. One of the important effects of the copper-based antineoplastic agents is changing the metabolism of cancer cells which causes different response between normal and cancer cells [11, 15]. It is worthy to note that the normal function of cells is critically dependent on the copper concentration in them. Copper homeostasis and metabolism are also crucial to various human cancers [15-17]. In comparing the cancerous tissues and normal tissues it is revealed that the concentration level of copper is very high in cancerous tissues. Therefore, cancer cells may represent a suitable, selective target for copper-based agents [15, 18]. Also, it has been established that copper compounds delay cell cycle progression, increase cell death in different cell cultures, and cause apoptosis in cultured mammalian cells which is considered to be crucial for drugs [19-21].

Herein, we synthesized an amino-alcohol ligand, namely; 2,6-bis-[(2-hydroxy ethylimino)methyl]-4-methylphenol (L^1) (Scheme 1) and investigated its self-assembly with copper (II) centers. The phenoxo group of the Schiff base ligand bridged metal centers and created a tetranuclear complex. This complex exhibited cytotoxicity effect against A549, Jurkat

and Raji cell lines. The interaction with BSA was also investigated by UV-Vis, fluorescence, and synchronous fluorescence spectroscopic techniques.

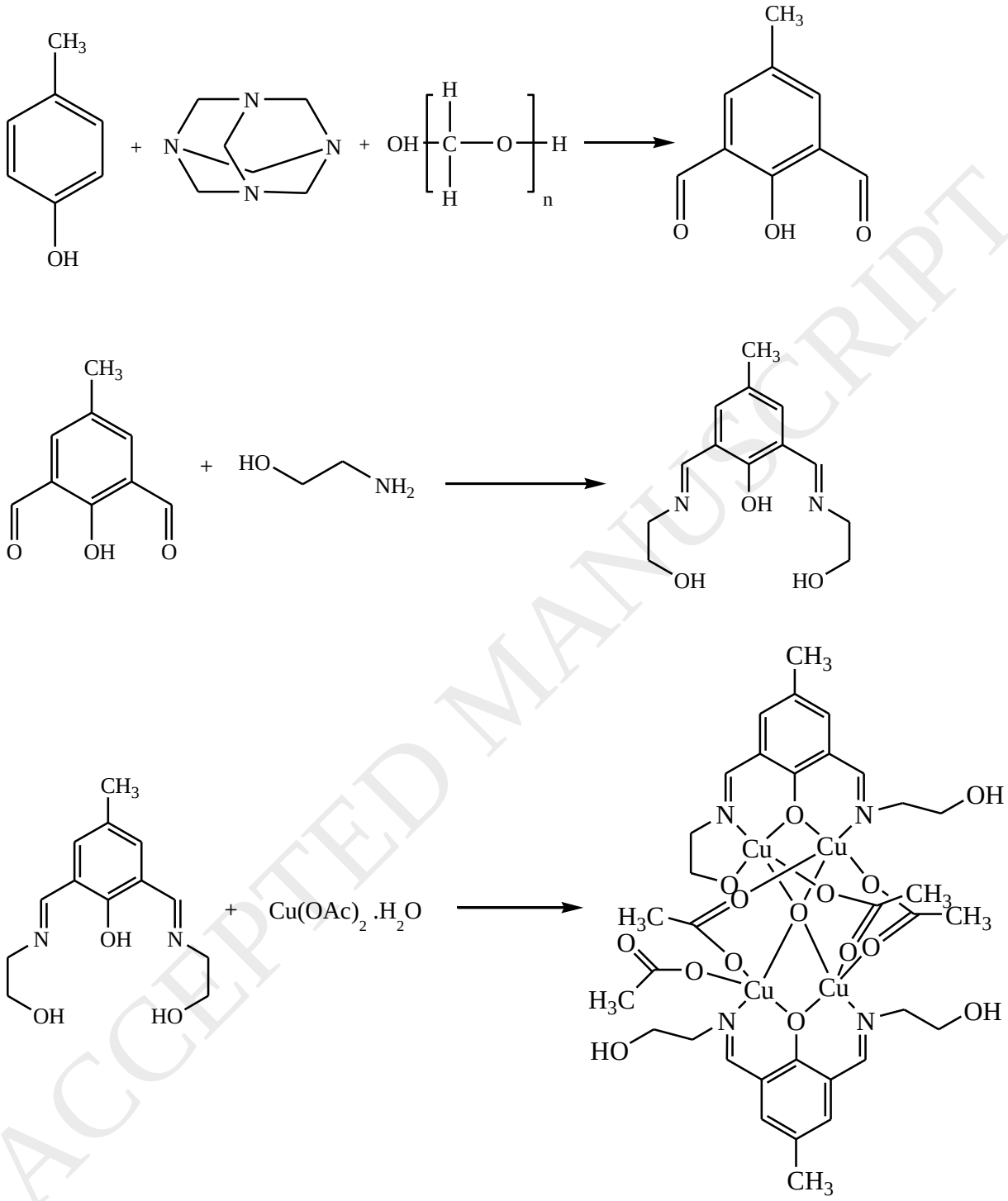

Scheme 1: Synthetic route of the tetranuclear copper (II) Schiff base cluster.

Experimental

Materials

Paraformaldehyde, phenylbutazone, 2-aminoethanol, bovine serum albumin (BSA), ibuprofen, hexamethylenetetramine, p-cresol, copper(II) acetate, methanol, ethanol, sulfuric acid, acetic acid, toluene, diethyl ether, n-hexane, chloroform, dimethylsulfoxide (DMSO), Tris-HCl buffer solution, NaCl, $CDCl_3$ and DMSO-d_6 for NMR spectroscopy, potassium bromide (KBr) for FT-IR spectroscopy were obtained from Sigma and Aldrich, Fluka and Merck.

Instruments

The NMR spectra were measured by Bruker Avance DPX 250 MHz spectrometer. Perkin-Elmer (LAMBDA 25) UV-Vis. spectrophotometer was used for UV-Vis. measurements which was equipped with LAUDA-ecoline-RE 104 thermostats. Shimadzu FT-IR 8300 infrared spectrophotometer and Thermo Finnigan-Flash 1200 were employed for FT-IR spectra and Elemental analysis (C.H.N.). Melting points of compounds were measured with BUCHI 535. X-ray diffraction measurements were made at 120K on a Gemini diffractometer of Rigaku Oxford Diffraction using the mirror-collimated CuKα radiation from a classical sealed X-ray tube, and CCD detector Atlas S2. All biological experiments were performed in triple distilled water at pH 7.4, 1 mM Tris buffer and 5 mM NaCl was used to create a biological medium. Variation in fluorescence and synchronous fluorescence spectra of the interactions were measured by a Perkin Elmer (LS 45) spectrofluorimeter.

Synthesis of 2,6-bis-[(2-hydroxyethylimino)methyl]-4-methylphenol (L^1)

The di-aldehyde precursor (2,6-diformyl-4-methylphenol) was prepared according to the procedure published by Verani et. al. [22]. To a methanolic solution of 2,6-diformyl-4-methylphenol (0.164 g, 1 mmol) was added 2-aminoethanol (0.12 ml, 2 mmol). The reaction mixture was refluxed for 3h after solvent evaporation; an orange product was collected by filtration, washed with a minimum volume of methanol and diethyl ether. The product was purified by recrystallization from methanol [23].(Fig. 1)

Yield: 0.18 g (72%); color: orange; m.p: 145 ºC; ^{1}H NMR (DMSO-d_6 , ppm): 14.36 (1H, s, OH^a), 8.54 (2H, s, HC=N), 7.50 (2H, s, Ar-H), 4.68 (2H, s, OH^b), 3.62 (8H, s, CH_2), 2.23 (3H, s, CH_3); FT-IR (KBr, cm^{-1}): 3348 (υ $_{O-H}$), 1635 (υ $_{C=N}$), 1604 and 1450 (υ $_{C=C}$), 1072 (υ $_{C-O}$); Elemental Analysis, Found (Calc.)%: $C_{13}H_{18}N_2O_3$ (MW=250 $g.mol^{-1}$) C: 62.46 (62.38); H: 7.55 (7.25); N: 11.30 (11.19)

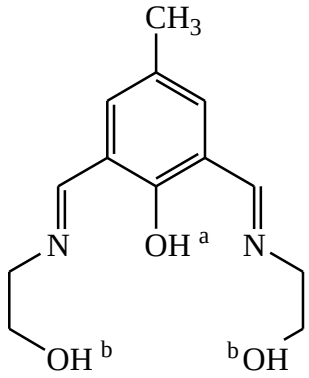

Fig. 1. The structure of 2,6-bis-[(2-hydroxyethylimino) methyl]-4-methylphenol (L^1)

Synthesis of $[Cu_4(L^1)_2(O)(OAc)_4].2H_2O$

To a methanolic solution (10 mL) of copper (II) acetate.H_2O (0.39 g, 2 mmol), a solution of L^1 (0.25 g, 1 mmol) in methanol was added slowly with continuous stirring at room temperature. The solution turned green immediately and stirred for 3h. The solution was kept for solvent evaporation. The green precipitate was filtered off and washed with diethyl ether. Green crystals suitable for X-ray crystallography were obtained in a solution of mixed solvents; methanol and n-hexane by the solvent penetration method; in which the complex completely dissolve in methanol while it is insoluble in n-hexane. Slow penetration of n-hexane in the methanolic solution of complex creates green crystals. (Fig. 2)

Yield: 0.27 g (26%); color: green; m.p: 175-186 ºC; FT-IR (KBr, cm^{-1}): 3417 (υ_{OH}), 1581 ($\upsilon_{C=N}$), 1627, 1455 ($\upsilon_{C=O\ diatomic\ bridge}$), 1627, 1411 ($\upsilon_{C=O\ one\ O\ attached\ to\ Cu}$), 1110 ($\upsilon_{C-O}$); Elemental Analysis, Found (Calc.)%: $C_{34}H_{43}Cu_4N_4O_{15}.2H_2O$ (MW=1037.94 $g.mol^{-1}$) C: 38.28 (39.34); H: 4.89 (4.56); N: 5.43 (5.40).

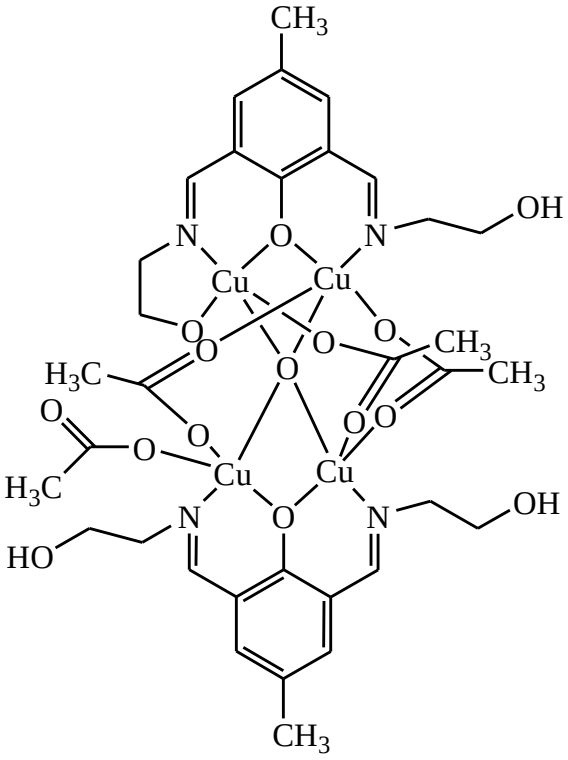

Fig. 2. The structure of $[Cu_4 (L_1)_2 (O) (OAc)_4]. 2H_2O$

X-ray crystallography

A saturated solution of the complex in a mixture of methanol and n-hexan solvents was allowed to evaporate at room temperature for two weeks and then green crystals of tetranuclear copper compound were obtained. The data were collected on Gemini diffractometer with Atlas CCD detector using mirror-collimated Cu-Kα radiation (λ = 1.54184 Å) and corrected for absorption using the CrysAlisPro software. The structure was solved by the charge-flipping method by program Superflip [24] and refined by full matrix least squares on F^2 with JANA 2006 program [25].

Protein-binding experiments

Fluorescence spectroscopy

Proteins reveal intrinsic fluorescence which makes the fluorescence spectroscopy a valid technique in the study of drug-protein interaction. BSA reveals an emission band at 260 nm thus wavelength range between 300-500 nm was selected to study the fluorescence emission spectra of BSA while the excitation wavelength was at 280 nm. The procedure was as follow: 2.5 mL of serum albumin solutions (7.2×10^{-8} M) (pH=7.4) was added to the quartz cell of 1 cm optical path and titrated by consecutive additions of complex (5×10^{-5} M). The equilibrium access

during 3 min after each injection, thus the change in fluorescence emission was measured at this point of time. As the complex revealed band around 260 nm, the complex band was eliminated by injecting equal amounts of complex solution to both reference cell and sample cell during titration.

UV-Vis spectroscopy

For the absorption titrations, free protein solution (BSA) (2×10^{-5}M) in Tris-HCl buffer (pH = 7.4) were poured into the cuvette, and the absorption in the absence and presence of the complex (2×10^{-3}M) was monitored in the wavelength range from 250 to 500 nm at 293, 298, 303 and 308 K.

Site marker competitive experiments

Bovine serum albumin contains several cavities, which can accommodate the whole or part of a metal complex. The preference of metal complex for particular cavity (or site) is examined by site marker competitive studies. Some specific compounds are used for this goal, for example, phenylbutazone that occupies site I of BSA is used as a site marker of the site I, and ibuprofen as a site marker of the site II of BSA. An effective procedure was supplied by mixing 2.5 mL BSA (7.2×10^{-8} M) and 10 μL phenylbutazone (or ibuprofen) (1.8×10^{-5} M in 50/50 V/V% water/acetone) and consequent titration with complex solution.

Synchronous fluorescence spectral measurements

This method consists in simultaneous scanning of the excitation and emission monochromator (at a fixed wavelength differences (Δλ) between them) for tyrosine and tryptophan amino acids. The addition of the complex causes some structural changes of BSA, and these structural changes effect on the synchronous fluorescence spectra at the wavelength interval Δλ =15 nm (tyrosine residues) and Δλ = 60 nm (tryptophan residue) of BSA [26].

The cytotoxicity experiments

The cytotoxic effects of the complex against two human leukemia\lymphoma cell lines (Jurkat and Raji) and a lung cancer cell line (A549) were measured by 3-(4,5-dimethylthiazol-2-yl)-2,5-diphenyltetrazolium bromide (MTT) assay as previously described [27]. The cell lines were grown in RPMI 1640 medium (Sigma, St. Louis, MO) supplemented with 10% fetal calf serum (Gibco, Berlin, Germany). Cells were cultured at 37ºC with 5% CO_2 and 95% humidity until confluent and after trypsinization (for A549) placed into new culture flasks. Jurkat and

Raji cells (15×10^3/well/100µL) and A549 cells (7.5×10^3 /well/100µL) were cultured in a 96-well plate in the presence of different concentrations of the complex (0.1–100 µg/mL). Cells treated only with dimethyl sulfoxide (solvent) at the same concentration used in the test wells was used as negative control and cells treated only with *cisplatin* considered as positive control. After 48 h, 10 µL MTT solution (5mg mL^{-1} in RPMI 1640 medium) was added to the plate and incubation was continued for 4 h. Finally, DMSO was added to dissolve the insoluble formazan and then the optical density (OD) at 570 nm and 630 nm (as a reference wavelength) was measured using a Bio-Tek microplate reader (ELx808, VT). The percentage of growth inhibition was calculated according to the following formula: [1– (OD of test/OD of negative)] × 100. The concentration of 50% cell inhibition (IC_{50}) values was determined using Curve Expert software.

Docking of the complex to BSA

In docking studies, the crystal structure of BSA (PDB ID: 3V03) was selected from the Brook-haven Protein Data Bank (http://www.pdb.org). This structure model is complete, based on data of good resolution, without any crystallized ligand.

Molecular docking of the complex in both two main sites of BSA was investigated using Molegro Virtual Docker (Moldock) software [28]. In Moldock, the units are arbitrary, and an ideal hydrogen bond contributes to the overall energy [28]. The energy based Moldock scoring function includes terms accounting for short range interactions such as hydrophobic, dispersion, or van der Waals, electrostatic interaction, loss of entropy upon ligand binding, hydrogen bonding and solvation. In this work, we have selected score as Moldock score [GRID], with GRID resolution of 0.30 Å, and for each docking calculation 10 different poses were requested. Parameters setting, pose generation and simplex evolution were selected as default settings.

Results and Discussion

Synthesis and characterization of the compounds

The synthesized ligand and complex were identified by FT-IR, ^{1}H NMR, electronic spectra and elemental analysis. Single crystals of the complex were prepared and X-ray crystallography was performed. The cluster complex was stable in atmosphere and soluble in water, DMSO, methanol and slightly soluble in methanol and insoluble in non-polar solvents.

The ^{1}H NMR spectrum of 2,6-diformyl-4-methylphenol was carried out in DMSO-d_6 and $CDCl_3$ (Figs. S1,2). The ^{1}H NMR spectrum of 2,6-bis-[(2-hydroxyethylimino)methyl]-4-

methylphenol in DMSO (Fig. S3) showed a singlet signal for OH^a at 14.36 ppm, a singlet signal for HC=N proton at 8.54 ppm, a singlet signal for aromatic protons at 7.50 ppm, a singlet signal for OH^b at 4.68 ppm, a singlet signal for CH_2 protons at 3.62 ppm and a singlet signal for the methyl protons at 2.23 ppm. For the distinction of OH signal one drop of D_2O was added to the DMSO-d_6 solution of the 2,6-bis-[(2-hydroxyethylimino) methyl]-4-methylphenol (Fig. S4). OH signals disappeared because of hydrogen binding with D_2O.

The FT-IR spectrum of 2,6-diformyl-4-methylphenol is revealed in Fig. S5. The Schiff base structure of 2,6-bis-[(2-hydroxyethylimino)methyl]-4-methylphenol was indicated by the presence of strong imine (C=N) bands at 1581 (Fig. S6) [29, 30].

In the complex (Fig. S7), the frequency of imine bond (C=N) is shifted to lower values, relative to the free ligand, indicating a decrease in the C=N bond order due to the coordination of the imine nitrogen to the metal and back bonding from the Cu(II) to the π^* orbital of azomethine group[31]. Shift toward lower values is also observed for (C-O) stretching vibration, again, as a result of coordination of the oxygen to the metal ion[32]. The vibration around 3450 cm^{-1} is assigned to the presence of lattice water[33] and medium-weak band at 2923 cm^{-1} is due the modes of vibrations of (C-H) groups [34]. The ring skeletal vibrations in the region of 1440–1465 were observed [35]. The M-O stretching vibration usually appears in the region 400-500 while M-N stretching vibration appears at around 410-580 cm^{-1} [29]. Thus, a close examination of the lower frequency infrared region helps to recognize M-O and M-N coordination in complex.

Two intense bands in the IR spectrum of complex observed at 1627 and around 1455 cm^{-1} were assigned to υ_{asym} (OCO) and υ_{sym} (OCO), respectively. The acetate coordination mode is assigned by the comparison of $\Delta\upsilon$ value of the acetate complex with the $\Delta\upsilon$ value of sodium acetate [31, 36, 37]. The $\Delta\upsilon$ = 172 cm^{-1} value of the acetate complex is almost equal to the value reported for sodium acetate ($\Delta\upsilon$ = 164 cm^{-1}) and indicated a diatomic bridging mode of acetate coordination that conforms to the structural data obtained by X-ray crystallography (vide infra). Two intense bands at 1627 and 1411 cm^{-1} for υ_{asym} (OCO) and υ_{sym} (OCO), (the $\Delta\upsilon$ = 216 cm^{-1} is bigger than that reported for sodium acetate) are related to the acetate that attached by one oxygen to the copper.

In the UV-Vis absorption spectrum of the complex (in Tris-HCl buffer, 2×10^{-5}M) phenyl and imine ($\pi\rightarrow\pi^*$) transitions, revealed two intense bands at 207 and 260 nm, respectively. Imine ($n\rightarrow\pi^*$) transition was recognized as a wide weaker absorption band at 378 nm. (Fig. S8)

X-ray structure analysis

A molecule of the tetranuclear copper complex is shown in Fig. 3. Crystallographic data and bond lengths and bond angles of the complex are listed in Tables 1, 2.

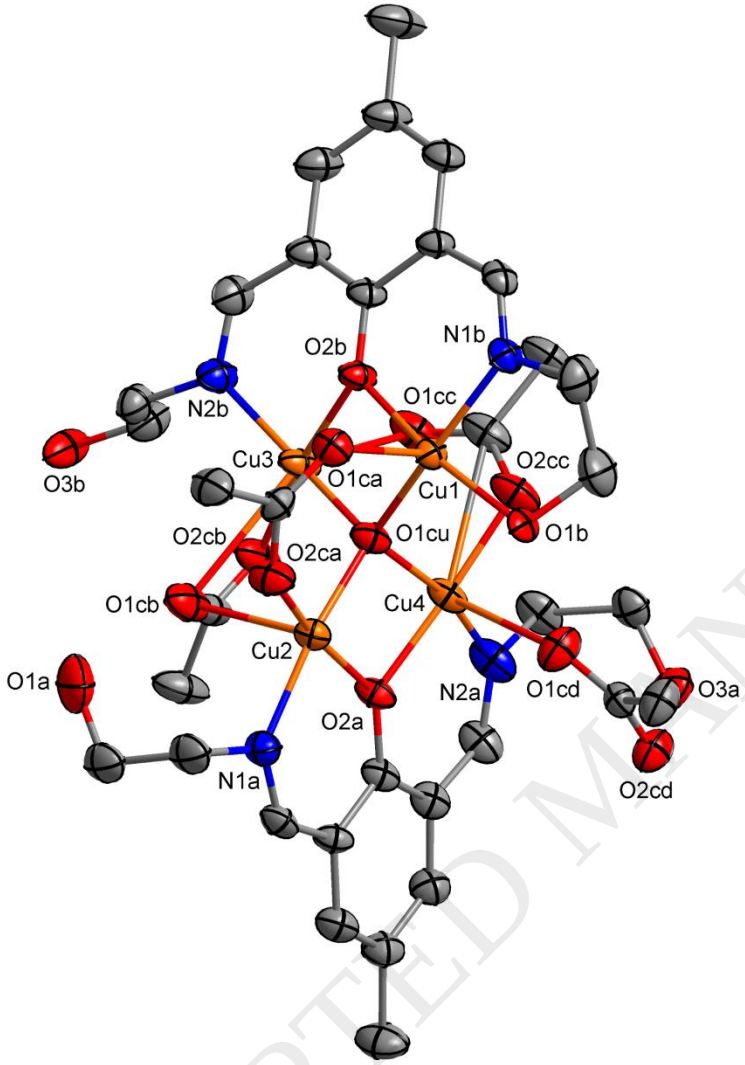

Fig. 3. A molecule of the tetranuclear copper complex. Labels of C, H atoms are omitted for clarity

Table 1. Crystal data and structure refinement for the complex

	Complex
Formula of refinement model	C34 H43 Cu4 N4 O15, 2(H2O), 0.497(O)
Temperature [K]	120
Crystal system	Triclinic
Space group	*P -1*
a [Å]	9.3168(5)
b [Å]	11.0701(7)
c [Å]	21.0231(8)
α [˚]	85.136(4)
β [˚]	86.012(4)
γ [˚]	71.594(5)
V[Å^3]	2047.8(2)
Z	2
D[gcm^{-3}]	1.696
μ [mm^{-1}]	3.025
F(000)	1076.0
R(F^2>3σ) (reflections)	0.0599(5651)
wR(F^2) (reflections)	0.1560(7162)

Table 2. Selected bond lengths (Å) and angles (°) for the complex

Bond angles (°)		Bond lengths (Å)	
Cu1,O1cu,Cu2	121.6(2)	Cu1-O1cu	1.902(4)
Cu1,O1cu,Cu3	100.8(2)	Cu1-O1b	2.001(6)
Cu1,O1cu,Cu4	111.3(2)	Cu1-O2b	1.969(3)
Cu2,O1cu,Cu3	116.0(2)	Cu1-N1b	1.959(5)
Cu2,O1cu,Cu4	101.8(2)	Cu1-O1ca	2.237(3)
		Cu2-O1cu	1.909(3)
Torsion angles (°)		Cu2-O2a	1.990(3)
		Cu2-N1a	1.989(3)
O2bCu1O1cuCu2	-128.1(2)	Cu2-O2ca	1.931(5)
O2bCu1O1cuCu3	1.7(1)	Cu2-O1cb	2.36(1)
O2bCu3O1cuCu2	131.6(2)	Cu3-O1cu	1.943(4)
O2bCu3O1cuCu4	-117.3(2)	Cu3-O2b	1.953(4)
O2aCu2O1cuCu1	-133.8(2)	Cu3-N2b	1.979(4)
O2aCu2O1cuCu4	-9.5(2)	Cu3-O2cb	1.95(2)
O2aCu4O1cuCu1	140.6(2)	Cu3-O1cc	2.484(4)
O2aCu4O1cuCu3	-111.5(2)	Cu4-O1cu	1.938(3)
		Cu4-O2a	1.960(4)
		Cu4-N2a	1.965(3)
		Cu4-O2cc	1.922(7)
		Cu4-O1cd	2.47(1)

The asymmetric unit of the copper(II) complex contains four Cu^{2+} cations with two 2,6-bis-[(2-hydroxyethylimino)methyl]-4-methylphenol (L^1) ligands and four acetate anions. L^1 ligand, in one side of the cluster, acts as N_2O_2 chelate while on the other side as N_2O chelate. The μ_2-O phenolic oxygens in both sides of the cluster make a bridge between two Cu centers (Cu(2),Cu(4) and Cu(1),Cu(3)); three acetates bridge two different Cu centers (Cu(3),Cu(4) and Cu(1),Cu(2) and Cu(2),Cu(3)) bidentately; and one acetate is coordinated to Cu(4) center monodentately. In the center of the structure, a μ_4-O connects four metals. Each Cu(II) center is five coordinated with one N atom and four O atoms (from acetates, central oxygen and ligand). Four Cu centers around the central μ_4-O display a distorted tetrahedral geometry (Fig. 4).

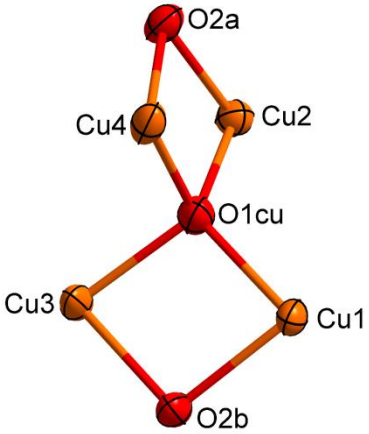

Fig. 4: Distorted tetrahedral geometry around central μ_4-O.

The coordination geometry of each penta-coordinated copper ion is distorted square pyramidal. To further investigate the distortion of the square pyramidal geometry a structural index parameter (τ) can be calculated for each Cu center. In the ideal square pyramidal geometry the metal center is displaced out of the square plane toward apical atom. Thus the angles between two opposite atoms (α & β) are < 180°. τ values as a geometric parameters for five-coordinate structures which define the degree of trigonality are calculated from $\tau = (\beta - \alpha)/60$. For perfect square pyramidal geometry τ is equal to zero and it became unity for perfect trigonal-bipyramidal geometry [38]. By comparing the τ values (τ_{Cu1}= 0.13, τ_{Cu2}= 0.002, τ_{Cu3}= 0.12, τ_{Cu4}= 0.12) it confirmed that the geometry around each Cu center is distorted square pyramid.

As usual for copper (II), the bond distances of the apical atoms are significantly longer than the bond distanced of the basal atoms for all the metal centers [8]. For Cu(2,3,4) centers: N, phenolic-O, central-O and one of the acetate-O create the basal plane (bond distances about 1.9 (Å)) and one of the acetate O creates the apical atom (bond distances about 2.36-2.48(Å)). For Cu(1) center: N, ligand-O, phenolic-O, central-O create the basal plane (bond distances about 1.9-2.0(Å)) while the apical O (O1ca) bond distance is 2.23(Å). (Fig.5)

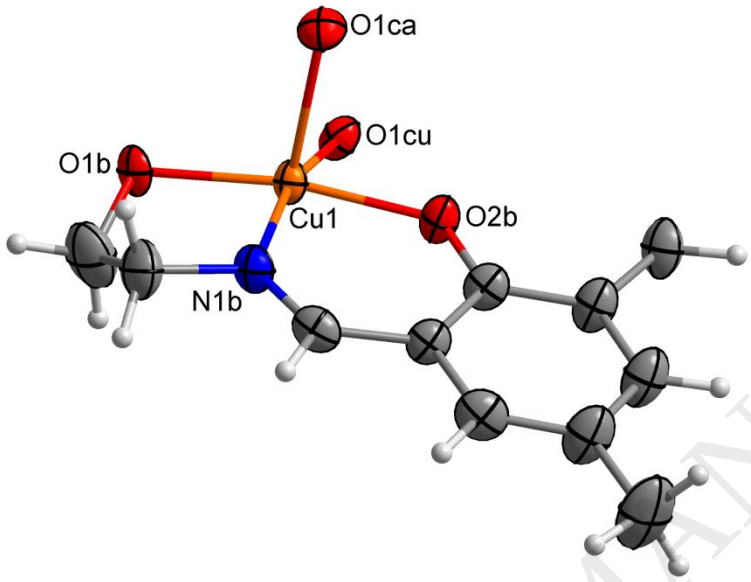

Fig. 5. Distorted square pyramidal geometry around Cu(1) center with the apical acetate oxygen and four basal atoms. Other atoms were omitted for the sake of clarity.

Fluorescence spectral studies

Proteins are known to display intrinsic fluorescence caused by the presence of three aromatic amino acids: tryptophan, tyrosine and phenylalanine. These three amino acids are relatively rare in proteins; for example, the amount of the dominant intrinsic fluorophore tryptophan is about 1 mole% in proteins. However, measurements of fluorescence titration spectra are highly sensitive and can be performed on dilute protein solutions. Because of the high sensitivity of tryptophan to its local environment, intrinsic protein fluorescence allows us to study binding interactions of proteins with different small molecules and monitor protein association reactions. Emission maximum intensity or quantum yield of tryptophan residues often change due to exposing to solvent or being in proximity of a quenching group [39].

Bovine serum albumin (BSA) is the most extensively studied serum albumin due to its structural homology with human serum albumin (HSA) [40]. The fluorescence spectra of the titration of BSA with various amount of complex are shown in Fig. 6. BSA has a strong

fluorescence emission peak around 345 nm after being excited at 280 nm.

The observed quenching of fluorescence emission intensity with a hypsochromic shift can be regarded to the formation of a new complex between tetra-nuclear Cu complex and BSA[40]. The hypsochromic shift is a sign that upon the interaction of complex with BSA the microenvironment around tryptophan residues becomes slightly hydrophobic [39].

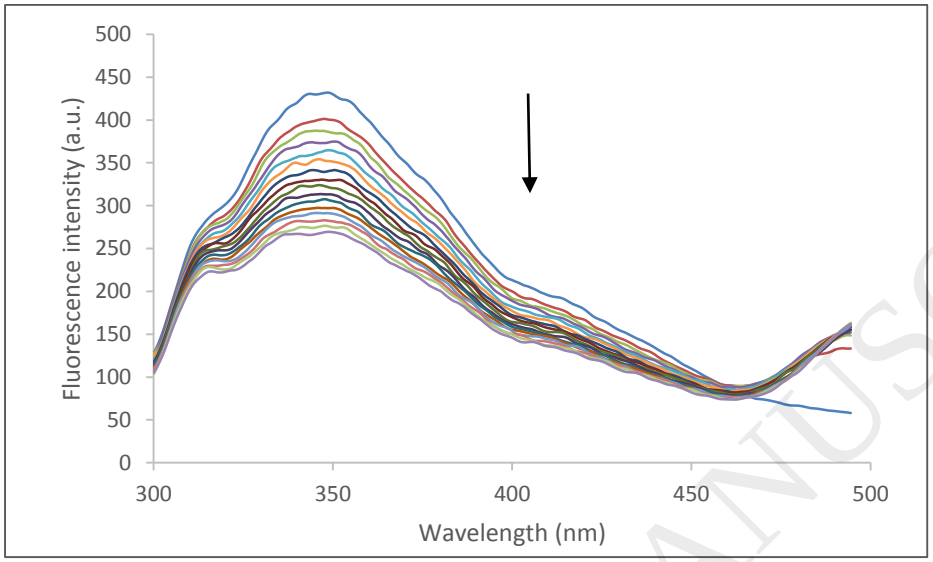

Fig. 6. The effect of complex on the fluorescence spectra of BSA (λ_{EX}=280),([complex] = 5×10^{-5} mol.L^{-1} / [BSA] = 7.2×10^{-8} mol.L^{-1}): 1.4, 2.8, 4.2, 5.6, 6.9, 8.3, 9.7, 11.1, 12.5, 13.9, 15.3, 16.7, 18.1, 19.4, 20.8; (T = 298 K)

The fluorescence quenching data can be analyzed by the Stern–Volmer Equation (1) [41],

$$\frac{F_0}{F} = 1 + K_{SV}[Q] = 1 + k_q \tau_0 [Q] \qquad (1)$$

Here F and F_0 are the fluorescence intensities in the presence and the absence of the quencher, respectively. K_{SV} is the Stern-Volmer quenching constant, [Q] is the concentration of the quencher, k_q is the bimolecular quenching constant, and τ_0 is the lifetime of the fluorophore in the absence of a quencher, which is 10^{-8} s for BSA[39].

The plot of F_0/F vs. [Q] gives the K_{SV} value. The Stern-Volmer quenching constant (K_{SV} = 3.8×10^{5}(M^{-1})) and quenching rate constant (k_q = 3.8×10^{13} ($M^{-1}s^{-1}$)) were obtained. The linear Stern-Volmer plot (Fig. 7) indicated that Equation (1) is applicable for the present system.

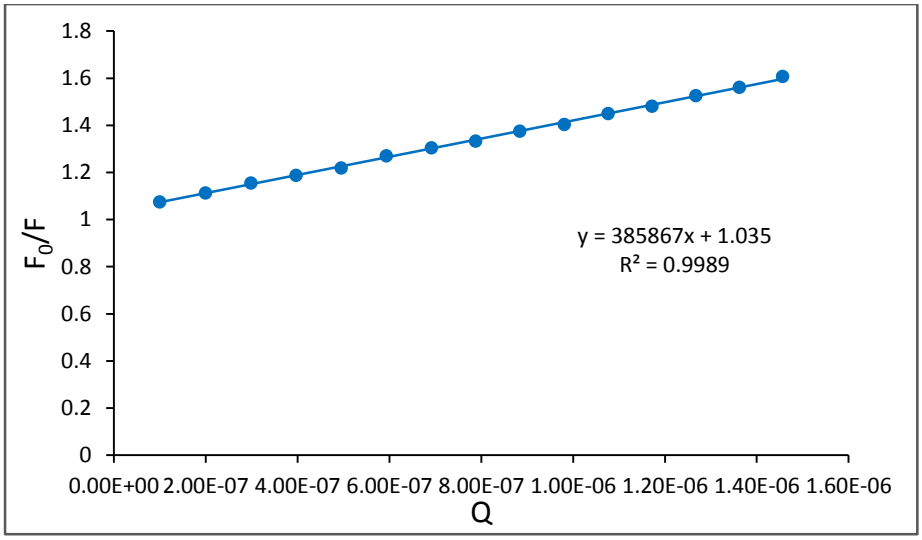

Fig. 7. The Stern–Volmer plot of complex (5×10^{-5} mol.L^{-1}) binding to BSA (7.2×10^{-8} mol.L^{-1}); λ_{Ex} = 280 nm, λ_{Em} = 345 nm.

Dynamic quenching and static quenching are two common fluorescence quenching mechanisms. The dynamic quenching mechanism takes part due to the excited state when the fluorophore and the quencher come into contact during the transient state. The static quenching refers to the ground state when the fluorophore and the quencher form a new complex. UV-Vis absorption spectroscopy is the easiest method used to determine the type of quenching[1, 42].

UV-Vis spectral studies

In order to distinguish between the quenching mechanisms of BSA by the complex, UV-Vis absorption spectra were recorded. The quenching mechanism which affects the excited states of the fluorophores is dynamic quenching. This mechanism induce no changes in the absorption spectra but static quenching which affect by fluorophore-quencher complex formation in the ground state induce changes in the absorption spectrum of fluorophore [40].

BSA has an absorption band at around 280 nm resulted from the aromatic amino acids (Trp, Tyr and Phe). Upon the addition of the complexes to the BSA, the absorption is enhanced (Fig. S9_and a slight blue shift occurs [44], manifesting there is an interaction between BSA and complex [43]. This result also indicated that the microenvironment of the three aromatic acid residues was altered and the interaction between the complex and BSA was mainly a static quenching mechanism [44].

The intrinsic binding constant, K_b for all the complex was determined from the spectral titration data using Equation (2) at four temperatures (293, 298, 303 and 308K) (Figs. 8, S10-

S12):

$$\frac{[complex]}{(\varepsilon_a - \varepsilon_f)} = \frac{[complex]}{(\varepsilon_b - \varepsilon_f)} + \frac{1}{K_b\,(\varepsilon_b - \varepsilon_f)} \quad (2)$$

Here [complex] is the concentration of complex, ε_a corresponds to the extinction coefficient observed (A_{obsd}/ [M]), ε_f corresponds to the extinction coefficient of the free compound, ε_b is the extinction coefficient of the compound when fully bound to BSA, and K_b is the intrinsic binding constant. The ratio of slope to intercept in the plot of [complex]/ ($\varepsilon_a - \varepsilon_f$) versus [complex] gave the value of K_b (Fig. 9). The K_b values are presented in Table 3.

Dynamic or static quenching mechanisms can also be distinguished by their dependence on temperature and viscosity, or by lifetime measurements. For dynamic interaction which mainly depends on diffusion, increasing temperature causes faster diffusion and hence higher dynamic quenching constants. On the other hand, in the static quenching mechanism, which refer to formation of a complex between a bio-macromolecule and the quencher in the ground state, increasing of temperature may cause the dissociation of weakly bound complexes and decrease of the static quenching constants [45]. By comparing K_b values at different temperatures (Table 3) it was clear that the K_b decreased with increasing the temperature thus a static quenching mechanism was confirmed.

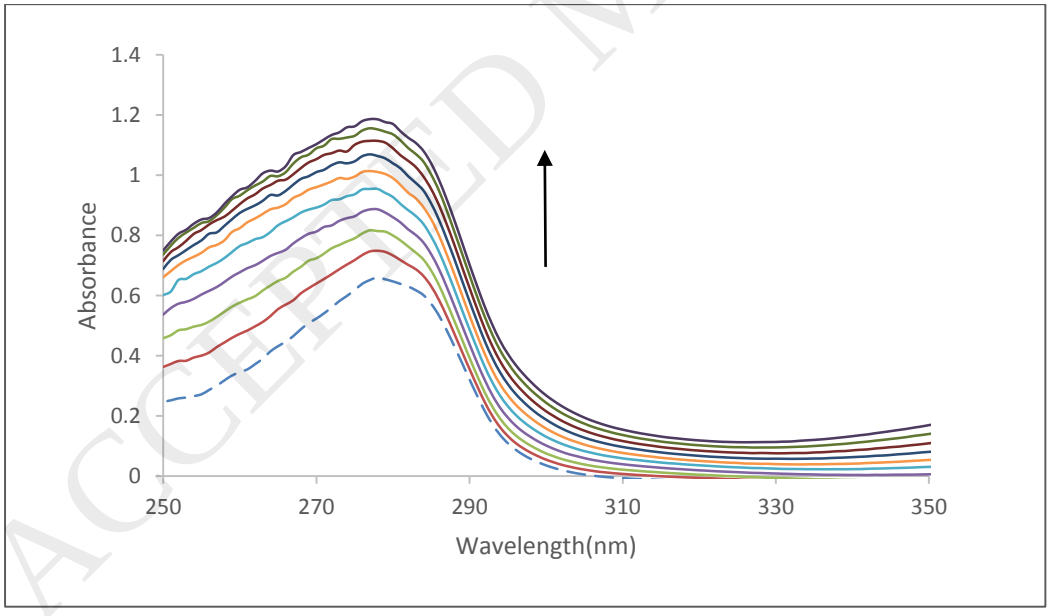

Fig. 8. Titration of BSA (2×10^{-5}M) (dot line) with various concentrations of complex (2×10^{-3}M) (0-45μL) at 20°C.

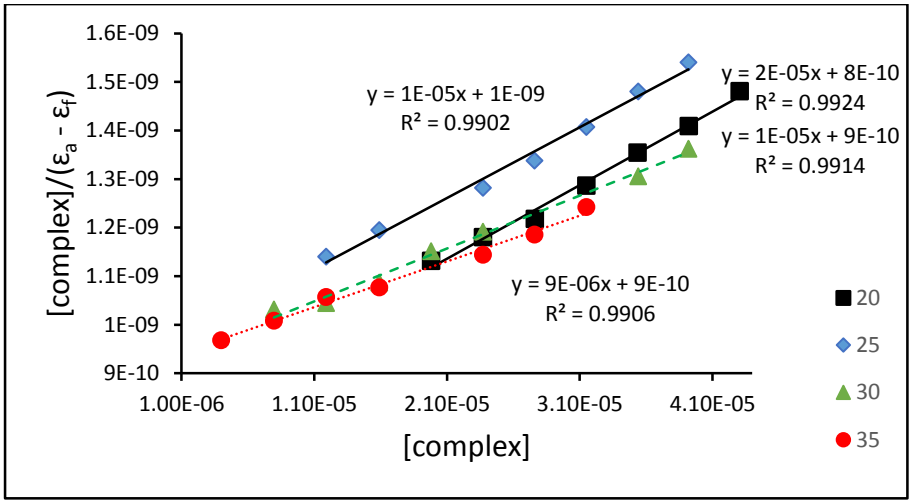

Fig. 9. The plot of [complex]/(ε_a - ε_f) versus [complex] at 20, 25, 30 and 35°C.

Thermodynamic parameters and binding modes

Four types of non-covalent interactions, namely hydrophobic interactions, electrostatic interactions, van der Waals forces and hydrogen bonds play an important role in the protein–drug binding. In order to elucidate the binding modes the thermodynamic parameters such as free energy change (ΔG), enthalpy change (ΔH) and entropy change (ΔS) are used, where ΔG reveals the possibility of the reaction, ΔH and ΔS values are used to calculate the acting forces. For small changes of the temperature, ΔH can be considered a constant. Then through the binding constant Kb , thermodynamic parameters can be calculated from van't Hoff Equation (3) and Equation (4) :[39, 46]

$$\ln K_b = -\frac{\Delta H}{RT} + \frac{\Delta S}{R} \quad (3)$$

Here K_b is the binding constant at the corresponding temperature and R is the gas constant.

$$\Delta G = \Delta H - T\Delta S \quad (4)$$

Resulting thermodynamic parameters are given in Table 3.

Table 3. Apparent binding constant and relative thermodynamic parameters for the interaction of complex with BSA at different temperatures.

Compounds	**T (K)**	**K_b (M^{-1})**	**R^2**	**ΔH (kJ mol^{-1})**	**ΔG (kJ mol^{-1})**	**ΔS (J mol^{-1} K^{-1})**
Complex	293	1.8×10^4	0.9924	-29.80 ±0.92	-23.89	-20.19 ±3.08
	298	1.5×10^4	0.9902		-23.78	
	303	1.2×10^4	0.9914		-23.68	
	308	1.0×10^4	0.9906		-23.58	

From the data given in Table 3, negative value of free energy (ΔG) supported the assertion that the binding process was spontaneous. Ross and Subramanian[47] have considered the signs and magnitudes of the thermodynamic parameters to elucidate various kinds of interactions that may take place in protein association processes. The negative ΔH and ΔS values indicated that van der Waals' forces and hydrogen bonds might play major roles in binding between complex and BSA[46].

Binding stoichiometry

The average aggregation number of BSA, <J>, which potentially could be induced by complex, can be determined by Equation (5).

$$1 - \frac{F}{F_0} = < J > \frac{[Q]}{[BSA]_0} \qquad (5)$$

Where F and F_0 are the fluorescence intensities in the presence and the absence of the quencher, respectively and [Q] is the concentration of the quencher, the slope (<J> = 0.0159) of the line presented in Fog. 10 is less than one, which indicated that the complex binding did not induce any aggregation in BSA molecules and accordingly proved the 1:1 stoichiometry for complex-BSA systems.

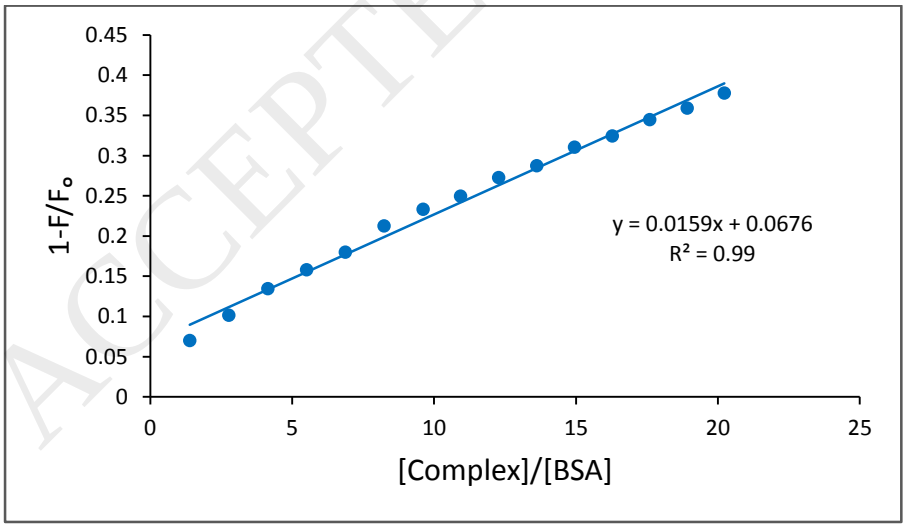

Fig. 10. Determination of the average aggregation number of BSA (<J>) in presence of complex. λ_{Ex} =280 nm, λ_{Em}=345 nm.(T=298 K)

Binding constants and the number of binding sites

For further investigation on the proposed static quenching interaction, the fluorescence intensity data were used to analyze the apparent binding constant (K_b) and the number of binding sites (n) by using Equation (6) [42]. This Equation calculates the equilibrium between free and bound small molecules when those bind independently to a set of equivalent sites on bio-macromolecules.

$$log\left(\frac{F_0 - F}{F}\right) = \log K_b + nlog[Q] \qquad (6)$$

Here, F_0 and F are the fluorescence intensities in the absence and presence of the quencher (complex), respectively; K_b is the binding constant of the compound with BSA; n is the number of binding sites per albumin molecules; and [Q] is the concentration of the quencher (complex). From the plot of log [(F_0 -F)/F] vs. log [Q] (Fig. 11), the binding constant (K_b =2.5×10^4 M^{-1}) and the number of binding sites (n = 0.796) were calculated. By considering the value of K_b, the distribution of the complex in protein can be estimated. The large K_b illustrated a strong binding between complex and BSA. The value of (n) was approximately equal to 1 which suggested that there was only one binding site for the complex on BSA molecule [42].

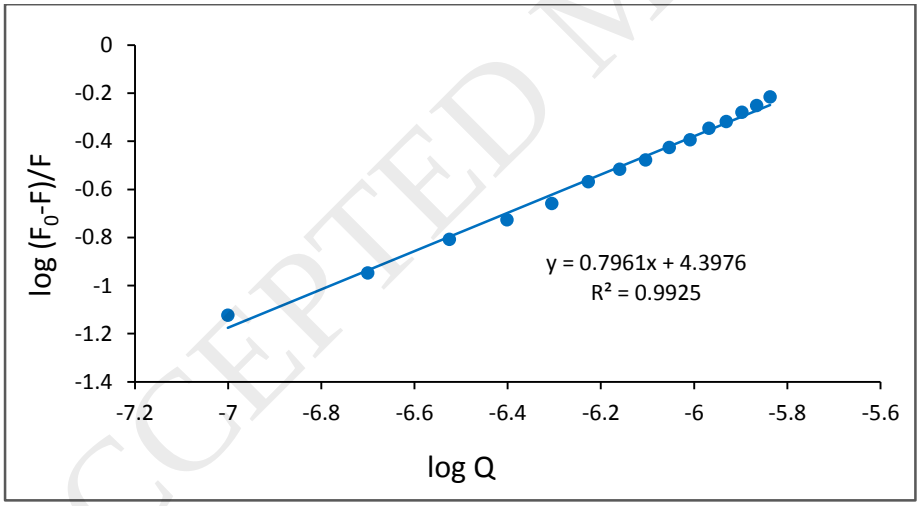

Fig. 11. Plot of log [(F_0-F)/F] vs. log[Q] for the complex

Site-selective binding of complex on BSA

In the molecular structure of Bovine serum albumin two main sites has been recognized for drugs binding: site I, in which the tryptophan residue is located for drug binding, and site II, in

which the tyrosine residue is located for drug-BSA interaction. The former showed affinity for warfarin, phenylbutazone, etc., whereas the binding pocket of the latter is well suited for ibuprofen, diazepam, fluofenamic acid, etc. In order to identify the binding site of the complex to BSA, displacement experiments were performed with phenylbutazone and ibuprofen as site markers for site I and site II of BSA, respectively [48], by monitoring the changes in the fluorescence of the ternary mixtures of complex (5×10^{-5} mol.L^{-1})(0-45μL), BSA(7.2×10^{-8} mol.L^{-1}) and site marker(1.8×10^{-5} mol.L^{-1}) (Fig. 12). The binding constants in Table 4 revealed that after addition of complex, K_b (the binding constant of complex-BSA) value of ibuprofen-BSA mixture was remarkably small, while K_b in the phenylbutazone-BSA mixture remained almost the same compared to a pure BSA solution [49]. These results revealed that the complex tended to occupy site II which was occupied by ibuprofen molecules, and the complex couldn't win in this competitive binding reaction thus causing the small K_b .

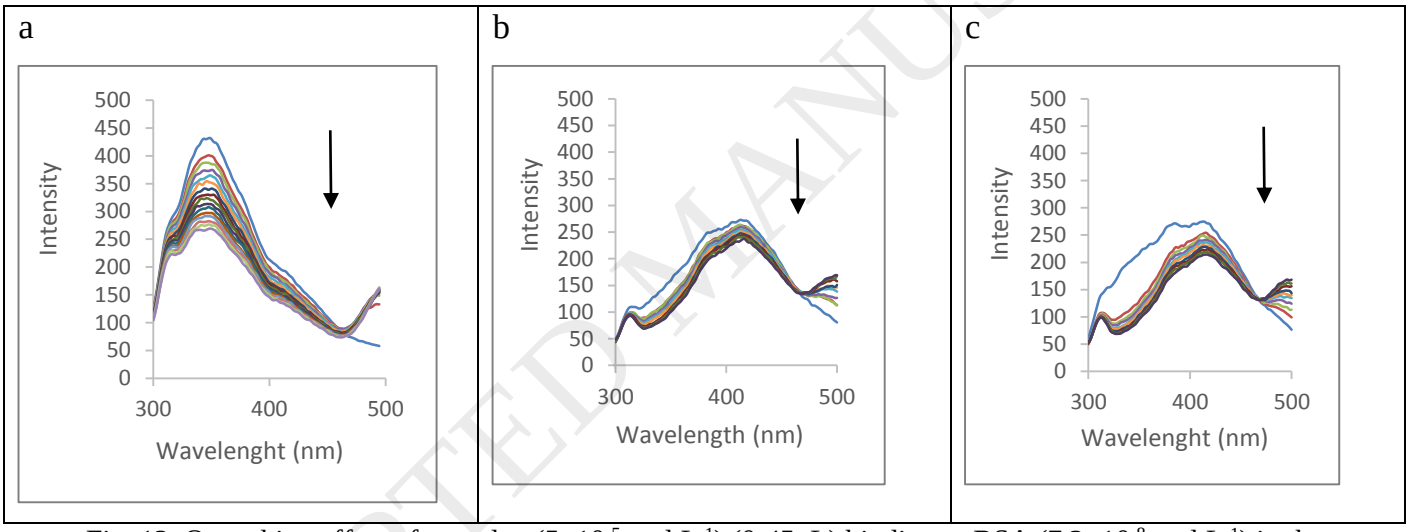

Fig. 12. Quenching effect of complex (5×10^{-5} mol.L^{-1}) (0-45μL) binding to BSA (7.2×10^{-8} mol.L^{-1}) in the a) absence of site marker, b) presence of phenylbutazone (1.8×10^{-5} mol.L^{-1}) and c) presence of ibuprofen (1.8×10^{-5} mol.L^{-1}).

Table 4. Binding constants of competitive experiment of complex-BSA system.

Complex	**Site marker**	**K_b (M^{-1})**	**R^2**
Complex	Without	2.498×10^4	0.9925
	Ibuprofen	0.211×10^4	0.9933
	Phenylbutazone	2.191×10^4	0.9965

Energy transfer and binding distance between complex and BSA

FRET (Förster resonance energy transfer) is a spectroscopic method used for estimating the proximity and relative angular orientation of fluorophores. FRET has been recognized as a "spectroscopic ruler" for measuring the distance between molecules in the biological and macromolecular systems. Resonance energy transfer takes place when the fluorescence emission band of donor overlaps with the excitation band of acceptor when they are in 2-8 nm distance[50, 51]. For the occurrence of Förster's resonance energy transfer (FRET) from donor to acceptor the following conditions must be fulfilled: (1) donor must be a fluorophore; (2) the fluorescence emission spectrum of the donor and UV–vis absorption spectrum of the acceptor must be sufficiently overlapped; (3) the distance between the donor and the acceptor must be within 2–8 nm[52]. Here the donor is BSA and the acceptor is the complex.

Using Förster theory (FRET) the distance between Complex and BSA could be calculated by Equation (7):

$$E = \frac{R_0^6}{R_0^6 + r^6} = 1 - \frac{F}{F_0} \tag{7}$$

Here E is the efficiency of transfer between the donor and the acceptor, F and F_0 are the fluorescence intensities of biomolecule (donor) in the presence and absence of acceptor (complex), r is the donor–acceptor distance and R_0 is the critical distance where the transfer efficiency is 50% calculated by using Equation (8):

$$R_0^6 = 8.8 \times 10^{-25} K^2 N^{-4} \Phi J \tag{8}$$

In Equation (8) K^2 is the spatial orientation factor related to the geometry of the donor and acceptor of dipoles, taking the value of 2/3 for random orientation as in fluid solution, N is the averaged refracted index of the medium in the wavelength range where spectral overlap is significant, taking the value of 1.336 for the average refracted index of water and organics, Φ is the fluorescence quantum yield of the donor taking the value of 0.118 for the fluorescence quantum yield of tryptophan [52], J is the effect of the spectral overlap between the emission spectrum of the donor and the absorption spectrum of the acceptor, which could be calculated by using Equation (9):

$$J = \frac{\int_0^\infty F(\lambda)\varepsilon(\lambda)\lambda^4 d\lambda}{\int_0^\infty F(\lambda) d\lambda} \tag{9}$$

Here F(λ) is the corrected fluorescence intensity of the donor in the wavelength range of λ to (l+Δλ) and ε(λ) is the molar extinction coefficient of the acceptor at λ.

The emission spectrum of BSA overlaps with the absorption spectrum of the complex in the wavelength range of 300 to 450 nm (Fig. 13). This considerable overlap forms the basis of FRET. Thus, the Förster's non-radiative energy transfer theory can be used to determine the distance between the amino acid residues on protein and the complex in the binding site[53]. By using Equations 7-9 the values $J = 2.62\times10^{-15}$ (cm^3 L mol^{-1}), E = 0.38, R_0 = 2.02nm and the binding distance r = 2.19 nm were calculated. The value of r is less than 8 nm, and $0.5R_0 < r < 1.5R_0$, indicating the energy transfer from BSA to the complex occurred with high probability [54-56].

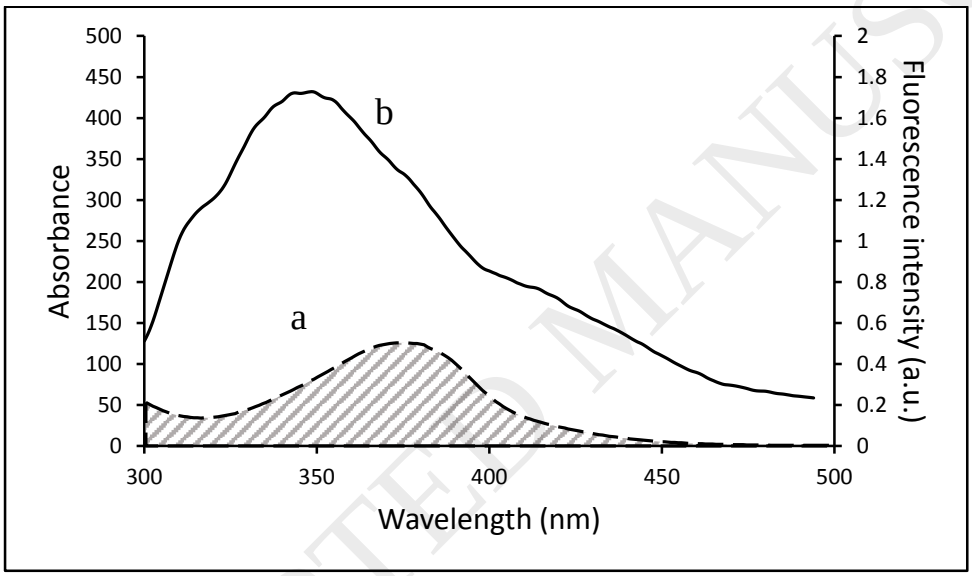

Fig. 13. Spectral overlap of (a) the absorption spectrum of complex (2×10^{-5} mol.L^{-1}) with(b) the BSA (7.2×10^{-8} mol.L^{-1}) fluorescence spectrum.

Synchronous fluorescence spectroscopic studies

Synchronous fluorescence spectra provide detailed information about the molecular microenvironment, particularly in the vicinity of the fluorophore in BSA [57]. In synchronous fluorescence spectroscopy, the difference between excitation and emission wavelengths ($\Delta\lambda = \lambda_{em} - \lambda_{ex}$) reflects the spectra of a different nature of chromophores. The large Δλ value (60 nm) is characteristic of tryptophan residue and a small Δλ value (15 nm) is characteristic of tyrosine [58]. Shift in the position of the maximum emission wavelength (λ_{max}) corresponds to changes

in the polarity around the chromophore molecule. The red shift of the maximum emission wavelength indicates an increasing polarity of the surrounding environment, a lower hydrophobicity and a looser structure of BSA, and vice versa[52].

The effect of the complex on the synchronous fluorescence spectra of BSA is shown in Fig. 14. In the synchronous fluorescence spectra at Δλ=15 nm for BSA, with increasing the concentrations of complex a decrease in fluorescence intensity at 282 nm with slight red shift of 1 or 2 nm was observed, which suggested a more polar (or less hydrophobic) environment of tyrosine residues. The synchronous fluorescence spectra of BSA at Δλ=60 nm exhibited a decrease in fluorescence intensity at 280 nm without any appreciable shift in the position of the band which indicated that there was no change of the microenvironment of tryptophan residues [46]. It was in accordance with the results of the site selective studies mentioned above.

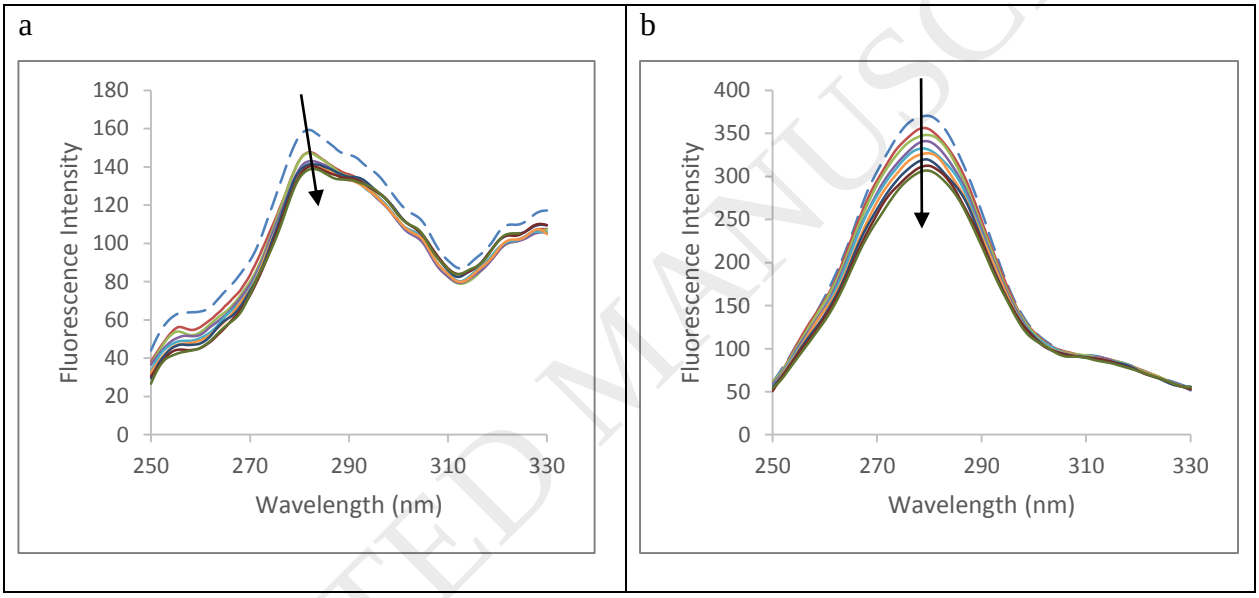

Figure 14. Synchronous fluorescence spectra of BSA (7.2×10^{-8} mol.L^{-1}) with Δλ=15nm (a) and Δλ=60nm (b) in the absence (dashed lines) and presence of complex (5×10^{-5} mol.L^{-1}) (0-40μL) (solid lines).

Inhibitory effects of the complex on various cancer cell lines

The antineoplastic activities of metal Schiff base complexes have been already established [59-61]. In the present study, the synthetic Schiff base complex was tested for its inhibitory effects on the growth of Jurkat human T cell leukemia, Raji Burkitt's lymphoma and A549 lung carcinoma cell lines as the target. The cell lines were treated with various concentrations of the complex to measure the cytotoxicity. Analysis of data showed a remarkable growth inhibitory

effect of the complex on all three cell lines. The Raji (IC_{50}, 9.8 μg/mL) and Jurkat (IC_{50}, 20.4 μg/mL) leukemia/lymphoma cells were more sensitive to the complex than the A549 solid tumor cells (IC_{50}, 48.4 μg/mL).

The IC_{50} values of *cis-platin* (as reference) for A549 cell line was 79.4 μg/mL, for Jurkat was 25 μg/mL and for Raji cells was 30 μg/mL.

Molecular docking study

The BSA molecule is made up of three homologous domains: domain I (residues 1–195), II (196–383) and III (384–585) that are divided into nine loops (L1–L9) by 17 disulfide bridges. Each domain is composed of two sub-domains (A and B) (Fig. 15).[62]

In the present study, the MVD program [63] was chosen to obtain the binding mode of the complex at the active site of BSA. The ranked results are reported in Table 5, showing that the best ranked result was obtained for site II of BSA. As shown in Fig. 16(a) the complex is inserted into the hydrophobic residues of site II (subdomain IIIA). The binding energy for the complex to BSA was found to be −198.276. These results are in agreement with those obtained by the experimental method. According to the Fig. 16(b) the complex is surrounded by a number of amino acid residues, namely: Ala489, Arg409, Arg484, Asn385, Asn390, Gln389, Gln393, Glu382, Ile387, Leu386, Leu490, Lys413, Phe487, Pro383, Pro485, Ser488, and Thr491. Non-coordinated OH groups of the complex could create H-bonding between the complex and some amino-acid residues of BSA. The main H-bonding interactions are collected in Table 6.

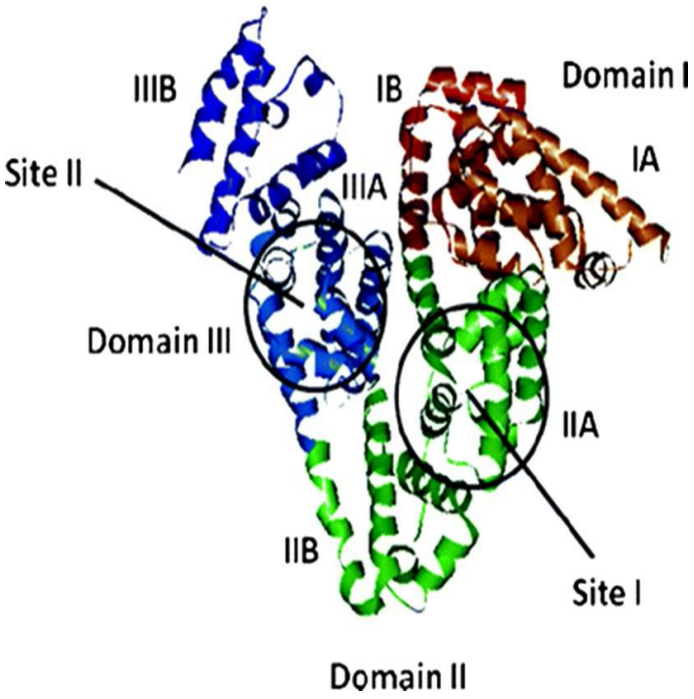

Figure 15. The structure of BSA

Table 5: Ranked results of the docking of the complex in site I and site II of BSA.

Rank	Mol Dock Score	
	Site I	Site II
1	-183.896	**-198.276**
2	-176.502	-191.27
3	-173.262	-175.719
4	-171.421	-174.68
5	-171.314	-170.997
6	-169.474	-169.085
7	-156.631	-165.172
8	-155.65	-156.596
9	-152.507	-152.96
10	-149.138	-142.378

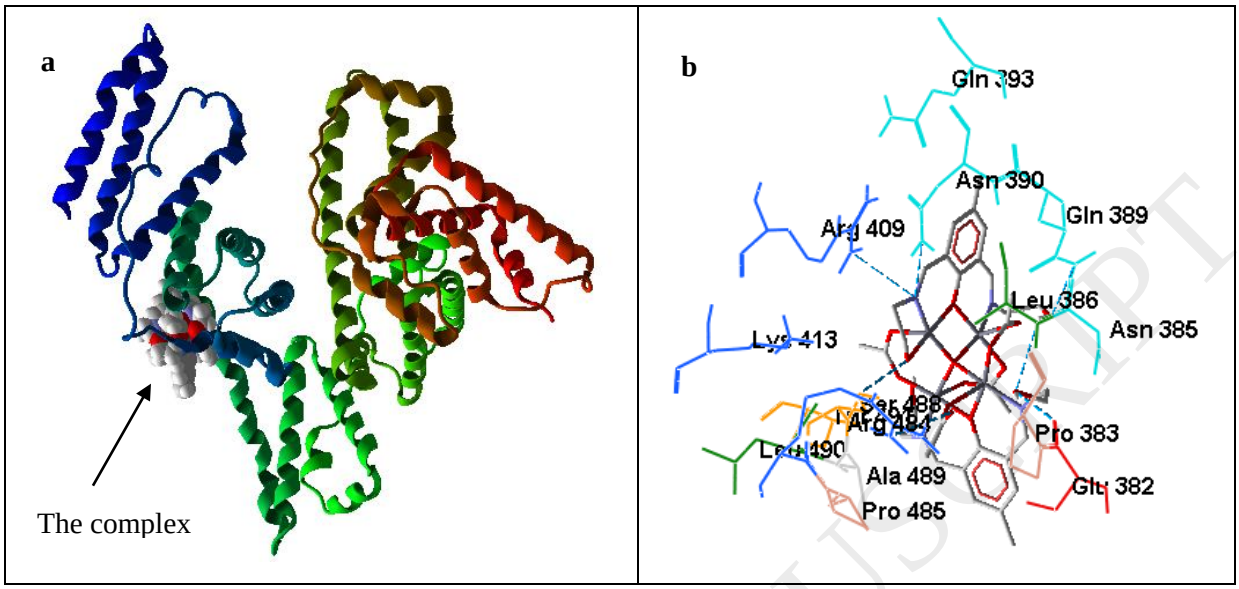

Figure 16: (a) The docking pose of the complex with BSA (b) the amino acid residues which surrounding the complex

Table 6: The main H-bonding between the amino-acids of BSA and complex

Hydrogen bond interaction	
Arg409	With N atom of ligand
Asn390	With N atom of ligand
Ser488	With O atom of ligand
Gln389	With OH group
Glu382	With OH group
Leu386	With OH group
Arg484	With OH group

Conclusion

A new tetranuclear copper (II) Schiff base complex was synthesized from 2,6-diformyl-4-methylphenol and 2-aminoethanol and copper(II) acetate as a metal source. The output of the synthesis was a tetranuclear water-soluble copper (II) cluster. The ligand and acetate ions bridged Cu(II) centers and arranged them in a distorted tetrahedral geometry around one central oxygen atom. The complex was characterized by elemental analysis, FT-IR, ^{1}H NMR and UV-Vis spectroscopy, and X-ray structure analysis. Some spectroscopic methods such as absorption, fluorescence and synchronous fluorescence spectroscopy were used to investigate the binding interaction of the complex with BSA. By the fluorescent titration the quenching rate constant were calculated by Stern-Volmer equation ($K_{SV} = 3.8\times10^{5}(M^{-1})$). Competitive binding experiments also revealed that the complex was located in site II of serum albumin. From the Förster energy transfer theory, the probability of the transfer efficiency of energy and the distance between the complex and protein were r = 2.19 nm.

Using the synchronous fluorescence spectroscopy, it was concluded that the interaction of complex with albumins did not change the conformation of tryptophan microenvironment, while the hydrophobicity near the tyrosine residues was changed.

The binding constants (K_b) were calculated from the UV-Vis spectroscopy in four different temperatures. The negative ΔH and ΔS values indicated that van der Waals' forces and hydrogen bonds were important in binding between complex and BSA and ΔG value indicated that the binding process is spontaneous.

Finally, the complex was examined for its anticancer activity against three human Jurkat, Raji and A549 tumor cell lines as the target. According to IC_{50} values, the results suggested that this complex might be a potential anticancer agent.

Acknowledgements

We are grateful to the Shiraz university research council for its financial support. The crystallographic part was supported by the project 18-10504S of the Czech Science Foundation using instruments of the ASTRA lab established within the Operation program Prague Competitiveness - project CZ.2.16/3.1.00/24510.

Supplementary material

CCDC 1544390 contains the supplementary crystallographic data for this paper. These data can be obtained free of charge from The Cambridge Crystallographic Data Centre via www.ccdc.cam.ac.uk/data_request/cif.

References

[1] M. Niu, Z. Li, H. Li, X. Li, J. Dou, S. Wang, DNA/protein interaction, cytotoxic activity and magnetic properties of amino-alcohol Schiff base derived Cu (II)/Ni (II) metal complexes: influence of the nuclearity and metal ions, RSC Adv., 5 (2015) 37085-37095.
[2] K. Das, T.K. Mondal, E. Garribba, M. Fondo, C. Sinha, A. Datta, Phenoxo bridged tetranuclear copper (II) and dinuclear zinc (II) complexes of 2, 6-diformyl-4-methylphenol-di (benzoylhydrazone): Synthesis, structure, spectra and magnetism, Inorg. Chim. Acta, 413 (2014) 194-202.
[3] V.H. Crawford, H.W. Richardson, J.R. Wasson, D.J. Hodgson, W.E. Hatfield, Relation between the singlet-triplet splitting and the copper-oxygen-copper bridge angle in hydroxo-bridged copper dimers, Inorg. Chem., 15 (1976) 2107-2110.
[4] E. Ruiz, P. Alemany, S. Alvarez, J. Cano, Toward the prediction of magnetic coupling in molecular systems: hydroxo-and alkoxo-bridged Cu (II) binuclear complexes, J. Am. Chem. Soc., 119 (1997) 1297-1303.
[5] W. Haase, Exchange interactions in tetranuclear copper (ii) complexes, J. Mol. Catal., 23 (1984) 331-340.
[6] E. Ruiz, A. Rodríguez-Fortea, P. Alemany, S. Alvarez, Density functional study of the exchange coupling in distorted cubane complexes containing the Cu 4 O 4 core, Polyhedron, 20 (2001) 1323-1327.
[7] A. Arbuse, M. Font, M.A. Martínez, X. Fontrodona, M.J. Prieto, V. Moreno, X. Sala, A. Llobet, DNA-cleavage induced by new macrocyclic Schiff base dinuclear Cu (I) complexes containing pyridyl pendant arms, Inorg. Chem., 48 (2009) 11098-11107.
[8] S. Majumder, S. Sarkar, S. Sasmal, E.C. Sãnudo, S. Mohanta, Heterobridged dinuclear, tetranuclear, dinuclear-based 1-D, and heptanuclear-based 1-D complexes of copper (II) derived from a dinucleating ligand: syntheses, structures, magnetochemistry, spectroscopy, and catecholase activity, Inorg. Chem., 50 (2011) 7540-7554.
[9] H. Liu, X. Shi, M. Xu, Z. Li, L. Huang, D. Bai, Z. Zeng, Transition metal complexes of 2, 6-di ((phenazonyl-4-imino) methyl)-4-methylphenol: Structure and biological evaluation, Eur. J. Med. Chem., 46 (2011) 1638-1647.
[10] S. Tardito, O. Bussolati, F. Gaccioli, R. Gatti, S. Guizzardi, J. Uggeri, L. Marchio, M. Lanfranchi, R. Franchi-Gazzola, Non-apoptotic programmed cell death induced by a copper (II) complex in human fibrosarcoma cells, Histochem. Cell Biol., 126 (2006) 473-482.
[11] C. Santini, M. Pellei, V. Gandin, M. Porchia, F. Tisato, C. Marzano, Advances in copper complexes as anticancer agents, Chem. Rev., 114 (2013) 815-862.
[12] D. Desbouis, I.P. Troitsky, M.J. Belousoff, L. Spiccia, B. Graham, Copper (II), zinc (II) and nickel (II) complexes as nuclease mimetics, Coord. Chem. Rev., 256 (2012) 897-937.
[13] L. Marcélis, J. Ghesquière, K. Garnir, A. Kirsch-De Mesmaeker, C. Moucheron, Photo-oxidizing Ru II complexes and light: Targeting biomolecules via photoadditions, Coord. Chem. Rev., 256 (2012) 1569-1582.
[14] C. Marzano, M. Pellei, F. Tisato, C. Santini, Copper complexes as anticancer agents, Anticancer Agents Med. Chem., 9 (2009) 185-211.
[15] W. Wan, R. Zhang, M. Ma, Y. Zhou, Monolithic aerogel photocatalysts: a review, J. Mater. Chem., (2017).
[16] M.C. Linder, J.R. Moor, K. Wright, Ceruloplasmin Assays In Diagnosis and Treatment of Human Lung, Breast, and Gastrointestinal Cancers 2 3 4, J. Natl. Cancer Inst., 67 (1981) 263-275.
[17] M. Diez, F. Cerdà, M. Arroyo, J. Balibrea, Use of the copper/zinc ratio in the diagnosis of lung cancer, Cancer, 63 (1989) 726-730.
[18] F. Tisato, C. Marzano, M. Porchia, M. Pellei, C. Santini, Copper in diseases and treatments, and copper-based anticancer strategies, Med. Res. Rev., 30 (2010) 708-749.
[19] E.R. Jamieson, S.J. Lippard, Structure, recognition, and processing of cisplatin− DNA adducts, Chem. Rev., 99 (1999) 2467-2498.

[20] S. Tardito, O. Bussolati, M. Maffini, M. Tegoni, M. Giannetto, V. Dall'Asta, R. Franchi-Gazzola, M. Lanfranchi, M.A. Pellinghelli, C. Mucchino, Thioamido coordination in a thioxo-1, 2, 4-triazole copper (II) complex enhances nonapoptotic programmed cell death associated with copper accumulation and oxidative stress in human cancer cells, J. Med. Chem., 50 (2007) 1916-1924.
[21] A. Paul, R.K. Gupta, M. Dubey, G. Sharma, B. Koch, G. Hundal, M.S. Hundal, D.S. Pandey, Potential apoptosis inducing agents based on a new benzimidazole schiff base ligand and its dicopper (II) complex, RSC Adv., 4 (2014) 41228-41236.
[22] C.N. Verani, E. Rentschler, T. Weyhermüller, E. Bill, P. Chaudhuri, Exchange coupling in a bis (heterodinuclear)[Cu II Ni II] 2 and a linear heterotrinuclear complex Co III Cu II Ni II. Synthesis, structures and properties, J. Chem. Soc., Dalton Trans., (2000) 251-258.
[23] D. Mandal, M. Chauhan, F. Arjmand, G. Aromí, D. Ray, Interaction with DNA of a heteronuclear [Na2Cu4] coordination cluster obtained from the assembly of two hydroxo-bridged [Cu II 2] units by a dimeric sodium nitrate template, Dalton Trans., (2009) 9183-9191.
[24] L. Palatinus, G. Chapuis, SUPERFLIP–a computer program for the solution of crystal structures by charge flipping in arbitrary dimensions, J. Appl. Crystallogr., 40 (2007) 786-790.
[25] V. Petříček, M. Dušek, L. Palatinus, Crystallographic computing system JANA2006: general features, Z. Kristallog. – Cryst. Mater., 229 (2014) 345-352.
[26] E. Burstein, N. Vedenkina, M. Ivkova, Fluorescence and the location of tryptophan residues in protein molecules, Photochem. Photobiol., 18 (1973) 263-279.
[27] Z. Amirghofran, M. Bahmani, A. Azadmehr, K. Javidnia, Anticancer effects of various Iranian native medicinal plants on human tumor cell lines, Neoplasma, 53 (2005) 428-433.
[28] R. Thomsen, M.H. Christensen, MolDock: a new technique for high-accuracy molecular docking, J. Med. Chem., 49 (2006) 3315-3321.
[29] D.X. West, A.A. Nassar, F.A. El-Saied, M.I. Ayad, Cobalt (II) complexes with 2-aminoacetophenone N (4)-substituted thiosemicarbazones, Transition Met. Chem., 24 (1999) 617-621.
[30] M. Tümer, H. Köksal, M.K. Sener, S. Serin, Antimicrobial activity studies of the binuclear metal complexes derived from tridentate Schiff base ligands, Transition Met. Chem., 24 (1999) 414-420.
[31] S. Meghdadi, K. Mereiter, V. Langer, A. Amiri, R.S. Erami, A.M. Alshima'a, M. Amirnasr, Synthesis, X-ray crystal structure, and electrochemistry of copper (II) complexes of a new tridentate unsymmetrical Schiff base ligand and its hydrolytically rearranged isomer, Inorg. Chim. Acta, 385 (2012) 31-38.
[32] M. Tümer, H. Köksal, S. Serin, M. Dig, Antimicrobial activity studies of mononuclear and binuclear mixed-ligand copper (II) complexes derived from Schiff base ligands and 1, 10-phenanthroline, Transition Met. Chem., 24 (1999) 13-17.
[33] I.A. Data, V.P. Tautomerism, I.S.B. Lengths, I.E. van der Waals Radii, V.B. Angles, H.V.S.B. Strengths, V.F. Constants, V. Torsion, X. Aromaticity, I.F.E.-C. Chart, The Chemist's Companion: A Handbook of Practical Data, Techniques, and References, (1972).
[34] G.G. Mohamed, Z.H.A. El-Wahab, Mixed ligand complexes of bis (phenylimine) Schiff base ligands incorporating pyridinium moiety: Synthesis, characterization and antibacterial activity, Spectrochim. Acta A, 61 (2005) 1059-1068.
[35] Y.-L. Zhang, W.-J. Ruan, X.-J. Zhao, H.-G. Wang, Z.-A. Zhu, Synthesis and characterization of axial coordination cobalt (III) complexes containing chiral Salen ligands, Polyhedron, 22 (2003) 1535-1545.
[36] G. Deacon, R. Phillips, Relationships between the carbon-oxygen stretching frequencies of carboxylato complexes and the type of carboxylate coordination, Coord. Chem. Rev., 33 (1980) 227-250.
[37] K. Nakamoto, Infrared and Raman spectra of inorganic and coordination compounds, Wiley Online Library, 1986.
[38] A.W. Addison, T.N. Rao, J. Reedijk, J. van Rijn, G.C. Verschoor, Synthesis, structure, and spectroscopic properties of copper (II) compounds containing nitrogen–sulphur donor ligands; the crystal and molecular structure of aqua [1, 7-bis (N-methylbenzimidazol-2'-yl)-2, 6-dithiaheptane] copper (II) perchlorate, J. Chem. Soc., Dalton Trans., (1984) 1349-1356.

[39] R. Patel, M.U.H. Mir, J.K. Maurya, U.K. Singh, N. Maurya, A.B. Khan, A. Ali, Spectroscopic and molecular modelling analysis of the interaction between ethane-1, 2-diyl bis (N, N-dimethyl-N-hexadecylammoniumacetoxy) dichloride and bovine serum albumin, Luminescence, 30 (2015) 1233-1241.
[40] P. Sathyadevi, P. Krishnamoorthy, R.R. Butorac, A.H. Cowley, N. Dharmaraj, Synthesis of novel heterobimetallic copper (I) hydrazone Schiff base complexes: a comparative study on the effect of heterocyclic hydrazides towards interaction with DNA/protein, free radical scavenging and cytotoxicity, Metallomics, 4 (2012) 498-511.
[41] J. Lakowicz, Principles of fluorescence spectroscopy, 3rd edn Plenum Press, N.Y., (2006).
[42] M. Niu, M. Hong, S. Cheng, J. Dou, Effect of structure and composition of nickel (II) complexes with salicylidene Schiff base ligands on their DNA/protein interaction and cytotoxicity, J. Inorg. Biochem., 137 (2014) 101-108.
[43] Y. He, Y. Wang, L. Tang, H. Liu, W. Chen, Z. Zheng, G. Zou, Binding of puerarin to human serum albumin: a spectroscopic analysis and molecular docking, J. Fluoresc, 18 (2008) 433-442.
[44] Q. Wei, J. Dong, P. Zhao, M. Li, F. Cheng, J. Kong, L. Li, DNA binding, BSA interaction and SOD activity of two new nickel (II) complexes with glutamine Schiff base ligands, J. Photochem. Photobiol., B, 161 (2016) 355-367.
[45] H.-x. Zhang, S. Gao, X.-x. Yang, Synthesis of an octupolar compound and its biological effects on serum albumin, Mol. Biol. Rep., 36 (2009) 1405.
[46] Y.Z. Zhang, X.X. Chen, J. Dai, X.P. Zhang, Y.X. Liu, Y. Liu, Spectroscopic studies on the interaction of lanthanum (III) 2-oxo-propionic acid salicyloyl hydrazone complex with bovine serum albumin, Luminescence, 23 (2008) 150-156.
[47] P.D. Ross, S. Subramanian, Thermodynamics of protein association reactions: forces contributing to stability, Biochemistry, 20 (1981) 3096-3102.
[48] Q. Wei, J. Dong, P. Zhao, M. Li, F. Cheng, J. Kong, L. Li, DNA binding, BSA interaction and SOD activity of two new nickel(II) complexes with glutamine Schiff base ligands, J. Photochem. Photobiol., B, 161 (2016) 355-367.
[49] Y. Zhang, S. Shi, X. Chen, W. Zhang, K. Huang, M. Peng, Investigation on the interaction between ilaprazole and bovine serum albumin without or with different C-ring flavonoids from the viewpoint of food–drug interference, J. Agric. Food Chem., 59 (2011) 8499-8506.
[50] S. Bano, A. Mohd, A.A.P. Khan, K. Siddiqi, Complexation and mechanism of fluorescence quenching of telmisartan with Y (III) and Nd (III), J. Chem. Eng. Data, 55 (2010) 5759-5765.
[51] S.H. Choi, K. Pang, K. Kim, D.G. Churchill, Cu2+ Colorimetric Sensing and Fluorescence Enhancement and Hg2+ Fluorescence Diminution in “Scorpionate”-like Tetrathienyl-Substituted Boron−Dipyrrins, Inorg. Chem., 46 (2007) 10564-10577.
[52] Y. Xiang, F. Wu, Study of the interaction between a new Schiff-base complex and bovine serum albumin by fluorescence spectroscopy, Spectrochim. Acta A, 77 (2010) 430-436.
[53] H. Farrokhpour, H. Hadadzadeh, F. Darabi, F. Abyar, H.A. Rudbari, T. Ahmadi-Bagheri, A rare dihydroxo copper (II) complex with ciprofloxacin; a combined experimental and ONIOM computational study of the interaction of the complex with DNA and BSA, RSC Adv., 4 (2014) 35390-35404.
[54] B. Valeur, M.N. Berberan-Santos, Molecular fluorescence: principles and applications, John Wiley & Sons, 2012.
[55] F. Samari, M. Shamsipur, B. Hemmateenejad, T. Khayamian, S. Gharaghani, Investigation of the interaction between amodiaquine and human serum albumin by fluorescence spectroscopy and molecular modeling, Eur. J. Med. Chem., 54 (2012) 255-263.
[56] N. Shahabadi, M. Maghsudi, S. Rouhani, Study on the interaction of food colourant quinoline yellow with bovine serum albumin by spectroscopic techniques, Food Chem., 135 (2012) 1836-1841.
[57] T.-S. Kang, Z. Mao, C.-T. Ng, M. Wang, W. Wang, C. Wang, S.M.-Y. Lee, Y. Wang, C.-H. Leung, D.-L. Ma, Identification of an iridium (III)-based inhibitor of tumor necrosis factor-α, J. Med. Chem., 59 (2016) 4026-4031.

[58] P. Krishnamoorthy, P. Sathyadevi, R.R. Butorac, A.H. Cowley, N.S. Bhuvanesh, N. Dharmaraj, Copper (I) and nickel (II) complexes with 1: 1 vs. 1: 2 coordination of ferrocenyl hydrazone ligands: Do the geometry and composition of complexes affect DNA binding/cleavage, protein binding, antioxidant and cytotoxic activities?, Dalton Trans., 41 (2012) 4423-4436.
[59] S.E.H. Etaiw, D.M.A. El-Aziz, E.H.A. El-Zaher, E.A. Ali, Synthesis, spectral, antimicrobial and antitumor assessment of Schiff base derived from 2-aminobenzothiazole and its transition metal complexes, Spectrochim. Acta A, 79 (2011) 1331-1337.
[60] X. Zhong, J. Yi, J. Sun, H.-L. Wei, W.-S. Liu, K.-B. Yu, Synthesis and crystal structure of some transition metal complexes with a novel bis-Schiff base ligand and their antitumor activities, Eur. J. Med. Chem., 41 (2006) 1090-1092.
[61] Z.-Y. Yang, R.-D. Yang, F.-S. Li, K.-B. Yu, Crystal structure and antitumor activity of some rare earth metal complexes with Schiff base, Polyhedron, 19 (2000) 2599-2604.
[62] J. Ao, L. Gao, T. Yuan, G. Jiang, Interaction mechanisms between organic UV filters and bovine serum albumin as determined by comprehensive spectroscopy exploration and molecular docking, Chemosphere, 119 (2015) 590-600.
[63] B. Hemmateenejad, M. Shamsipur, F. Samari, T. Khayamian, M. Ebrahimi, Z. Rezaei, Combined fluorescence spectroscopy and molecular modeling studies on the interaction between harmalol and human serum albumin, J. Pharm. Biomed. Anal., 67 (2012) 201-208.